Physical properties of the $Ce_2MAl_7Ge_4$ heavy-fermion compounds (M = Co, Ir, Ni, Pd)

N. J. Ghimire,[1,*] S. K. Cary,[2] S. Eley,[1] N. A. Wakeham,[1] P. F. S. Rosa,[1] T. Albrecht-Schmitt,[2] Y. Lee,[3] M. Janoschek,[1] C. M. Brown,[4] L. Civale,[1] J. D. Thompson,[1] F. Ronning,[1] and E. D. Bauer[1]

[1]*Los Alamos National Laboratory, Los Alamos, New Mexico 87545, USA*

[2]*Department of Chemistry and Biochemistry, Florida State University, Tallahassee, Florida 32306, USA*

[3]*Center for Artificial Low Dimensional Electronic Systems, Institute for Basic Science, Department of Physics at POSTECH Pohang, Korea 790-784*

[4]*National Institute of Standards and Technology, Center for Neutron Research, Gaithersburg, Maryland 20878, USA*

(Received 1 October 2015; revised manuscript received 4 April 2016; published 23 May 2016)

We report the synthesis, crystal structure, and characterization by means of single-crystal x-ray diffraction, neutron powder diffraction, and magnetic, thermal, and transport measurements of the new heavy-fermion compounds $Ce_2MAl_7Ge_4$ (M = Co, Ir, Ni, Pd). These compounds crystallize in a noncentrosymmetric tetragonal space group $P\bar{4}2_1m$, consisting of layers of square nets of Ce atoms separated by Ge-Al and M-Al-Ge blocks. $Ce_2CoAl_7Ge_4$, $Ce_2IrAl_7Ge_4$, and $Ce_2NiAl_7Ge_4$ order magnetically below T_M = 1.8, 1.6, and 0.8 K, respectively. There is no evidence of magnetic ordering in $Ce_2PdAl_7Ge_4$ down to 0.4 K. The small amount of entropy released in the magnetic state of $Ce_2MAl_7Ge_4$ (M = Co, Ir, Ni) and the reduced specific heat jump at T_M suggest a strong Kondo interaction in these materials. $Ce_2PdAl_7Ge_4$ shows non-Fermi liquid behavior, possibly due to the presence of a nearby quantum critical point.

DOI: 10.1103/PhysRevB.93.205141

I. INTRODUCTION

In heavy-fermion materials, hybridization between f-electron and conduction-electron states gives rise to a large specific heat coefficient $C/T = \gamma$, often 100–1000 times that of ordinary metals (e.g., Cu) [1,2]. The ground state is determined by a balance of competing Kondo and *RKKY* interactions, which are both described by an exchange interaction $|\mathcal{J}|$ that characterizes the hybridization strength between f-electron/conduction-electron states, as proposed by Doniach [3]. When $|\mathcal{J}|$ is small, the *RKKY* interaction dominates and the system orders magnetically, but for large $|\mathcal{J}|$, the material behaves as a heavy Fermi liquid: $\gamma \sim$ const., magnetic susceptibility $\chi \sim$ const., and electrical resistivity $\rho \sim T^2$. When the *RKKY* and Kondo interactions become comparable, the magnetic phase transition is suppressed to zero temperature at a quantum critical point (QCP) [4–6]. Here, quantum fluctuations give rise to non-Fermi liquid (NFL) behavior in the physical properties, e.g., $C/T \sim -\ln(T)$ or $\sim T^{-n}$, $\chi \sim \ln(T)$ or $\sim T^{-n}$, and $\rho \sim T^n$ ($n < 2$), depending on the nature of the fluctuations. A dome of unconventional superconductivity often occurs in the vicinity of the quantum critical point, where the quantum fluctuations are strongest and presumably mediate the superconductivity [4,7]. To explore the interplay of superconductivity and magnetism near a QCP, attention has focused on several families of tetragonal Ce-based compounds. For example, superconductivity is observed near an antiferromagnetic quantum critical point in CeM_2X_2 (M = transition metal; X = Si, Ge) [8], the $Ce_mM_nIn_{3m+2n}$ family [9] (M = transition metal, m and n are the number of the $CeIn_3$ and MIn_2 building blocks, respectively), and noncentrosymmetric $CePt_3Si$ and $CeMX_3$ (M = transition metal; X = Si, Ge) compounds [10].

The local crystal-chemical environment influences the magnetic behavior of heavy-fermion materials [11]. When a rare-earth ion, like Ce, is placed within a particular crystal-chemical environment, the interactions with the surrounding ligands [e.g., crystalline electric field (CEF), hybridization] modify the free-ion $4f$ electron wave function and its electronic and magnetic properties. Conventional density functional theory (DFT) calculations, unfortunately, are unable to capture sufficiently the complexity of these interactions with the detail that is needed to predict their outcome [12,13]. To our knowledge, theory has not anticipated any material to exhibit heavy-fermion properties. Instead, progress in understanding the interplay between crystal structure and chemistry and in the discovery of interesting new heavy-fermion states has come from an iterative process of materials discovery, characterization, and theory/modeling. The materials mentioned above are good examples of this paradigm and have been particularly instructive because they each comprise a family in which interactions can be tuned systematically by the crystal-chemical environment of the Ce's $4f$ electron. Only after these materials were discovered did experimental and theoretical study show how interesting they were. A crystal-chemical lesson from them is that a fruitful direction to look for similarly interesting behaviors is to explore for new Ce-containing materials with symmetry lower than cubic and containing a transition metal as well as an element from IIIB or IVB columns in the periodic table. This lesson is born out in a more recent example of the quasi-two-dimensional $CeMAl_4Si_2$ family (M = Rh, Ir, Pt) in which nominally isoelectronic Rh and Ir members are moderately heavy-fermion antiferromagnets and nominally electron-doped M = Pt is ferromagnetic [14–16]. In the course of exploring the possible consequences of expanding the crystal lattice of this family by replacing Si with larger Ge, we discovered a family of quasi-two-dimensional $Ce_2MAl_7Ge_4$ (M = Co, Ir, Ni, Pd) compounds that, as we discuss, are interesting in their own right. Herein, we report the synthesis and physical characterization of single crystals of this family of compounds by means of x-ray diffraction, magnetization, electrical resistivity, and specific

*nghimire@lanl.gov

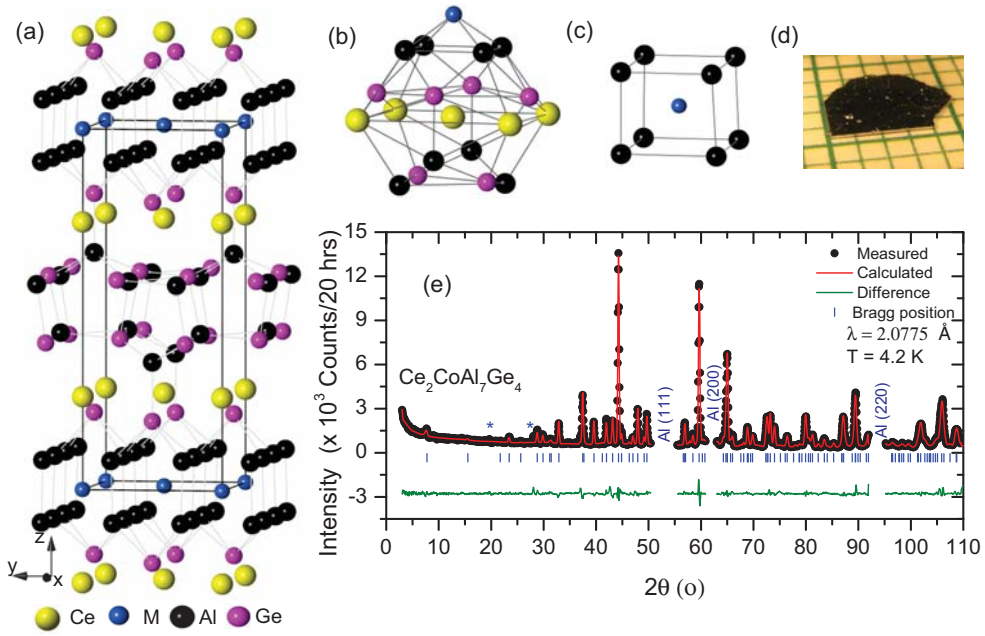

FIG. 1. (a) Crystal structure of $Ce_2MAl_7Ge_4$, (b) atomic environment of Ce, (c) atomic environment of M, (d) photo of a crystal of $Ce_2NiAl_7Ge_4$ on a 2 mm × 2 mm grid, and (e) Rietveld refinement of the neutron powder pattern of $Ce_2CoAl_7Ge_4$ measured above the magnetic transition temperature at $T = 4.2$ K. The Al peaks from the sample holder are excluded. The asterisks (∗) indicate unknown impurity peaks.

heat. Unlike the $CeMAl_4Si_2$ materials, these $Ce_2MAl_7Ge_4$ compounds crystallize in a noncentrosymmetric tetragonal space group $P\bar{4}2_1m$. This crystal-chemical environment leads to magnetic order below $T_M = 1.8$, 1.6, and 0.8 K in $Ce_2CoAl_7Ge_4$, $Ce_2IrAl_7Ge_4$, and $Ce_2NiAl_7Ge_4$, respectively. A large $4f$ contribution to the specific heat and the reduced entropy below T_M [∼0.2–0.3 Rln(2), where R is the gas constant] suggest a significant Kondo interaction in these three materials; the comparable Kondo and $RKKY$ energy scales indicate that the $Ce_2MAl_7Ge_4$ compounds are close to the magnetic/nonmagnetic boundary in the Doniach diagram [3]. $Ce_2PdAl_7Ge_4$ does not order magnetically and shows non-Fermi liquid behavior down to 0.4 K with the Sommerfeld coefficient reaching $\gamma \sim 1$ J/mol Ce K^2. There is no detectable superconductivity in the $Ce_2MAl_7Ge_4$ materials above 0.4 K.

II. EXPERIMENTAL DETAILS

Single crystals of $Ce_2MAl_7Ge_4$ (M = Co, Ir, Ni, Pd) were grown from an Al/Ge flux. First, $CeMGe_3$ was prepared by arc melting the stoichiometric composition on a water-cooled copper hearth under an argon atmosphere with a Zr getter. The arc-melted $CeMGe_3$ was mixed with $Al_{88}Ge_{12}$ in a ratio of 1:8 by weight and loaded into a 5-ml crucible. The crucible was sealed in a quartz ampoule under vacuum. The sealed ampoule was heated to 1100 °C in 6 h, homogenized at 1100 °C for 24 h, and then slowly cooled to 700 °C at the rate of 4 °C/h. Once the furnace reached 700 °C, the excess flux was decanted from the crystals using a centrifuge. Platelike crystals were obtained in all cases. Crystals as large as 8 × 6 × 0.3 mm were obtained [Fig. 1(d)]. Isostructural $La_2MAl_7Ge_4$ analogs were prepared by a similar method.

The crystal structure of the $Ce_2MAl_7Ge_4$ compounds was determined by single-crystal x-ray diffraction at room temperature. Large single crystals were isolated and broken into small fragments, which were then mounted on mitogen loops with immersion oil, and optically aligned on a Bruker D8 Quest x-ray diffractometer using a digital camera. Initial intensity measurements were performed using an IμS x-ray source (Mo $K\alpha$, $\lambda = 0.710\,73$ Å) with high-brilliance and high-performance focusing multilayered optics. Standard APEXII software was used for determination of the unit cells and data collection control. The intensities of reflections of a sphere were collected by a combination of multiple sets of exposures (frames). Each set had a different φ angle for the crystal and each exposure covered a range of 0.5° in ω. A total of 1464 frames were collected with an exposure time per frame of 5–10 s, depending on the sample. SAINT software was used for data integration, including Lorentz and polarization corrections. The large size of the crystals necessitated breaking the crystals and using small fragments as described above, which precludes a face-indexed numerical absorption correction.

Neutron powder diffraction experiments were carried out on $Ce_2CoAl_7Ge_4$ and $Ce_2NiAl_7Ge_4$ using the high-resolution powder diffractometer BT-1 at the NIST Center for Neutron Research [17]. A neutron wavelength of 2.077 5 Å was selected using a Ge(311) monochromator, which avoids higher-order contamination of the monochromated beam via its crystal symmetry. Powder samples were prepared by pulverizing single crystals. 2.4 grams of $Ce_2CoAl_7Ge_4$ and 3.0 grams of $Ce_2NiAl_7Ge_4$ were loaded in aluminum and copper cans, respectively. A diffraction pattern was collected for 20 h at 4.2 and 0.42 K for $Ce_2CoAl_7Ge_4$ and at 2, 0.5, and 0.137 K for $Ce_2NiAl_7Ge_4$. A Rietveld refinement of the crystal structure was carried out using the program FULLPROF [18].

The chemical composition of the $Ce_2MAl_7Ge_4$ single crystals was analyzed using a scanning electron microscope

TABLE I. Crystallographic data of $Ce_2MAl_7Ge_4$ (M = Co, Ir, Ni, Pd) determined by single-crystal x-ray diffraction.

Crystal system	Tetragonal			
Space group	$P\bar{4}2_1m$			
Temperature	296(2) K			
Wavelength	0.71073 Å			
Z formula units	2			
$2\theta_{min}$	2.65°			
$2\theta_{max}$	27.55°			
Index ranges	$-7 \leqslant h \leqslant 7, -7 \leqslant k \leqslant 7, -19 \leqslant l \leqslant 20$			
Compound	$Ce_2CoAl_7Ge_4$	$Ce_2IrAl_7Ge_4$	$Ce_2NiAl_7Ge_4$	$Ce_2PdAl_7Ge_4$
Formula weight	818.39	951.66	818.17	865.86
a (Å)	5.9158(3)	5.9786(4)	5.9343(3)	6.0070(4)
c (Å)	15.3635(19)	15.366(2)	15.2733(17)	15.2632(19)
Volume (Å^3)	537.67(8)	549.25(9)	537.86(7)	550.76(9)
Density (calculated)(g/cm^3)	5.055	5.754	5.052	5.221
μ (Mo Kα) (cm^{-1})	213.26	314.69	215.27	209.47
Goodness of fit on F^2	1.127	1.128	1.245	1.211
$R(F)$ for $F_o^2 > 2\sigma(F_o^2)$[a]	0.0171	0.0175	0.0186	0.0265
$R_w(F_o^2)$[b]	0.0422	0.0401	0.0459	0.0700

[a] $R(F) = \sum || F_o | - | F_c || / \sum | F_o |$.

[b] $R_w(F_o^2) = [\sum[w(F_o^2 - F_c^2)^2]/ \sum w F_o^4]^{1/2}$.

(SEM) with an energy-dispersive x-ray spectrometer (EDS). The atomic percentages of the $Ce_2MAl_7Ge_4$ compounds were determined to be: Ce, Co, Al, Ge = 14.22, 6.82, 49.93, 29.03; Ce, Ir, Al, Ge = 14.46, 7.31, 47.93, 30.30; Ce, Ni, Al, Ge = 14.60, 7.42, 48.13, 29.80; and Ce, Pd, Al, Ge = 14.49, 7.30, 47.71, 30.00. These values are within the expected uncertainty for the standardless measurements, fully consistent with the composition Ce:M:Al:Ge = 2:1:7:4, normalized to M, and with the site occupancies found in refinement of the x-ray diffraction measurements in the $P\bar{4}2_1m$ space group (see Appendix Tables VII–IX). The La analogs were also characterized by chemical composition analysis with similar results. dc magnetization measurements between 0.4 K and 350 K in magnetic fields up to $H = 70$ kOe were performed in a Quantum Design Magnetic Property Measurement System (MPMS). Electrical resistivity and specific heat capacity measurements of crystals were carried out in a Quantum Design Physical Property Measurement System (PPMS) down to 0.4 K and in magnetic fields up to 90 kOe. The heat capacity of the La compounds was measured down to 2 K. Electrical contacts for resistivity measurements were made by spot welding 25-μm-diameter Pt wires onto the sample so that resistivity was measured with current applied in the ab plane. The electrical resistivity of $Ce_2CoAl_7Ge_4$ and $Ce_2NiAl_7Ge_4$ was measured in an external field of 200 and 500 Oe, respectively, to suppress the superconductivity due to traces of Al-Ge impurities [19].

III. RESULTS

A. Crystal structure

Analysis of single-crystal x-ray diffraction patterns revealed that the compounds $Ce_2MAl_7Ge_4$ (M = Co, Ir, Ni, Pd) are isostructural and crystallize in a defect variant of the Sm_2NiGa_{12} structure type [20–22] with a noncentrosymmetric space group $P\bar{4}2_1m$ (no. 113). Any possible missed symmetry in the structure of the $Ce_2MAl_7Ge_4$ compounds was checked for using the PLATON software package [23] along with CHECKCIF, both of which indicated possible pseudosymmetry and a possible centrosymmetric space group of $P4/nmm$. However, the reduction of symmetry to the noncentrosymmetric, but not polar, $P\bar{4}2_1m$ space group is invoked by the differences in the Ce-Al vs Ce-Ge bond distances, which approximates, but does not equal, an n glide. Furthermore, the refinement in $P4/nmm$ is considerably poorer than in $P\bar{4}2_1m$ and also induces Al/Ge disorder that, upon refinement, leads to a formula inconsistent with the microprobe analysis described below. In addition, the thermal displacement parameters are unreasonable and in some cases nearly nonpositive definite in $P4/nmm$. All indications are that $P\bar{4}2_1m$ is the correct space group. Crystallographic Information Files (CIFs) are available from the Inorganic Crystal Structure Database (ICSD) [24].

The crystallographic data are presented in Table I and the fractional atomic coordinates and equivalent displacement parameters for $Ce_2CoAl_7Ge_4$ are given in Table II. (The atomic coordinates of the M = Ni, Pd, and Ir compounds are listed in Appendix Tables VII–IX). A unit cell of $Ce_2MAl_7Ge_4$ consists of four Ce atoms, two M atoms, 14 Al atoms, and eight Ge atoms (two formula units per unit cell, $Z = 2$). The crystallographically equivalent Ce atoms occupy the 4d Wyckoff position. The M atoms are also crystallographically equivalent, residing in 2a Wyckoff position. There are three crystallographically inequivalent Ge sites and four crystallographically inequivalent Al sites where Ge1, Ge2, and Ge3 occupy the 2c, 2c, and 4e Wyckoff positions and Al1, Al2, Al3, and Al4 occupy the 4e, 2c, 4e, and 4e Wyckoff positions, respectively. The atomic environment of Ce and M atoms constructed with atoms before the maximum gap [25] are

TABLE II. Atomic coordinates and equivalent displacement parameters (Å^2) for $Ce_2CoAl_7Ge_4$ determined by single-crystal x-ray diffraction at room temperature. U_{eq} is defined as one-third of the trace of the orthogonalized U^{ij} tensor.

Atom	Wyckoff	Occ.	x	y	z	U_{eq}
Co(1)	2*a*	1	0	0	0	0.005(1)
Ce(1)	4*d*	1	0	0	–0.2564(1)	0.006(1)
Ge(1)	2*c*	1	0.5	0	–0.2008(1)	0.008(1)
Ge(2)	2*c*	1	0	0.5	–0.1892(1)	0.008(1)
Ge(3)	4*e*	1	0.2810(1)	–0.2190(1)	–0.4124(1)	0.011(1)
Al(1)	4*e*	1	–0.2920(3)	–0.2080(3)	–0.4279(1)	0.007(1)
Al(2)	2*c*	1	0	-0.5	–0.3531(2)	0.009(1)
Al(3)	4*e*	1	–0.2557(2)	–0.2443(2)	–0.0835(2)	0.008(1)
Al(4)	4*e*	1	–0.7436(2)	–0.2436(2)	–0.0841(2)	0.010(1)

depicted in Figs. 1(b) and 1(c). Each Ce atom is surrounded by one M, eight Al, six Ge, and four Ce atoms with a coordination number of 19. Each M atom is surrounded by eight Al atoms in a nearly cubic environment. Thus, one may view the crystal structure as consisting of a planar square net of Ce atoms separated by M-Al-Ge and Al-Ge blocks alternating along the c axis, as shown in Fig. 1(a). The Ce-Ge and Ce-Al distances range from 3.1016(3) to 3.1640(6) Å and 3.3071(10) to 3.3816(19) Å, respectively.

The replacement of some Ge with Al within the local environment around Ce sites causes a reduction in the site symmetry from $2/m$ in Sm_2NiGa_{12} to simple twofold symmetry. However, the M sites are surrounded solely by Al in $Ce_2MAl_7Ge_4$ and have an increase in site symmetry to $\bar{4}$. Furthermore, though the Ge atoms are surrounded by both Al and Ce, the local environment around Al is remarkably complex and consists of close contacts with Ce, M, and Ge. The complexity of the local environment surrounding the Al centers also significantly contributes to the reduction in both the site and translational symmetry. The Al and Ge site symmetry is never greater than twofold in $Ce_2MAl_7Ge_4$, whereas two of the Ge sites in Sm_2NiGa_{12} reside on the $2/m$ positions.

A Rietveld refinement of the crystal structure of $Ce_2CoAl_7Ge_4$ based on the neutron powder pattern collected above the magnetic transition temperature at 4.2 K is depicted in Fig. 1(e). The Al peaks from the sample holder can were excluded from the refinement pattern. A similar refinement of the neutron powder pattern of $Ce_2NiAl_7Ge_4$ collected at 2 K was also performed. A crystal structure with space group $P\bar{4}2_1m$ determined by single-crystal x-ray diffraction as described above was used in the refinement in each case. The thermal parameters were held fixed to zero, assuming that the Debye-Waller factor at the measured temperatures is negligible. The results of the refinement are presented in Table III. In each sample, a few small peaks were not successfully indexed [as marked by asterisks in Fig. 1(e)] and are attributed to a small amount of an unknown impurity phase.

B. Magnetic properties

The magnetic susceptibility $\chi \equiv M/H$ for $H = 1.1$ kOe applied parallel and perpendicular to the crystallographic c axis of $Ce_2MAl_7Ge_4$ (M = Co, Ni, Ir, Pd) is displayed in Figs. 2(a)–2(d). For all of the compounds, below 5 K, χ measured perpendicular to the c axis is greater than that measured parallel to the c axis, indicating easy plane magnetic moments. The high temperature susceptibility shows Curie-Weiss behavior in all four compounds. A Curie-Weiss fit to the data of the form $\chi = C/(T - \theta_{CW})$, where $C = N_A\mu_{eff}^2/3k_B$ is the Curie constant, N_A is Avogadro's number, and k_B is the Boltzmann constant, shown in Figs. 3(a)–3(d), yields the effective moment μ_{eff} and Curie-Weiss temperature θ_{CW}, which are presented in Table IV. The polycrystalline average effective moment for $Ce_2CoAl_7Ge_4$, $Ce_2IrAl_7Ge_4$, $Ce_2NiAl_7Ge_4$, and $Ce_2PdAl_7Ge_4$ is 2.42, 2.42, 2.43, and 2.55 μ_B/Ce, consistent with Ce being in a Ce^{3+} state for which the expected moment is 2.54 μ_B. Moreover, these effective moments indicate that the transition metal M ions are nonmagnetic in $Ce_2MAl_7Ge_4$ (M = Co, Ni, Ir, Pd). In all of the compounds, the Curie-Weiss temperatures are negative, indicating overall antiferromagnetic (and/or Kondo) interactions. $Ce_2CoAl_7Ge_4$, $Ce_2NiAl_7Ge_4$, and $Ce_2IrAl_7Ge_4$ show a tendency towards saturation below 2 K, indicating that these compounds order magnetically. Given the large value of χ (>2 emu/mol Ce) at 0.45 K in the

TABLE III. Crystallographic parameters and agreement factors from a Rietveld refinement of the neutron powder pattern of $Ce_2CoAl_7Ge_4$ and $Ce_2NiAl_7Ge_4$ in space group $P\bar{4}2_1m$ with atomic coordinates given in Tables II and VIII, respectively.

	$Ce_2CoAl_7Ge_4$	$Ce_2NiAl_7Ge_4$
T (K)	4.2	2.0
λ (Å)	2.0775	2.0775
a (Å)	5.9053(8)	5.9188(2)
c (Å)	15.3314(8)	15.2354(7)
Bragg R factor	4.5	6.3
χ^2	4.0	4.8

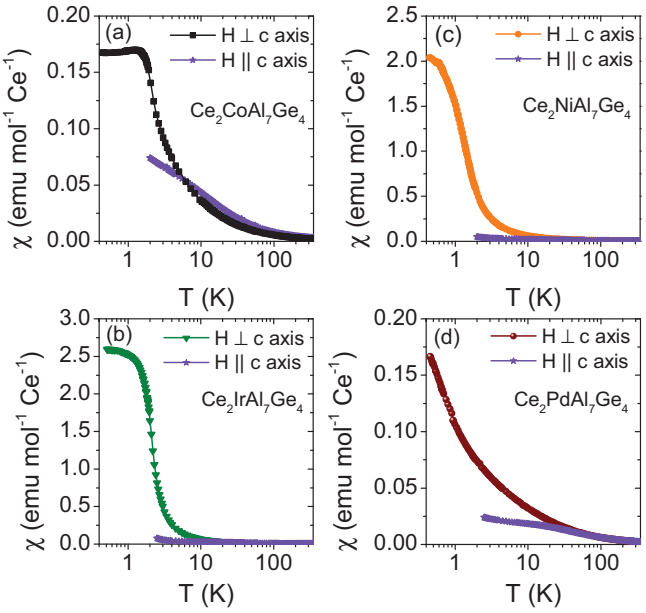

FIG. 2. Magnetic susceptibility χ of $Ce_2MAl_7Ge_4$ (M = Co, Ni, Ir, Pd) measured in an external magnetic field of $H = 1.1$ kOe applied parallel and perpendicular to the crystallographic c axis.

TABLE IV. Effective magnetic moment μ_{eff} and Curie-Weiss temperature θ_{CW} of $Ce_2MAl_7Ge_4$ compounds obtained from a Curie-Weiss fit to the high-temperature inverse susceptibility χ^{-1}.

Compound	$Ce_2CoAl_7Ge_4$	$Ce_2IrAl_7Ge_4$	$Ce_2NiAl_7Ge_4$	$Ce_2PdAl_7Ge_4$
μ_{eff} (H $\parallel$ c axis) (μ_B)	2.41[a]	2.41	2.50	2.54
μ_{eff} (H $\perp$ c axis) (μ_B)	2.42	2.42	2.39	2.56
μ_{eff} (poly. avg.) (μ_B)	2.42	2.42	2.43	2.55
θ_{CW} H $\parallel$ c axis (K)	3[a]	–3	–38	–34
θ_{CW} H $\perp$ c axis (K)	–37	–30	–11	–43
θ_{CW}(poly. avg.) (K)	–17	–21	–20	–40

[a]A modified Curie-Weiss law of the form $\chi = \chi_0 + C/(T - \theta_{\text{CW}})$ was used to determine these values.

ordered state for the M = Ni and Ir compounds, these materials likely order in a ferromagneticlike state. For $Ce_2CoAl_7Ge_4$ and $Ce_2PdAl_7Ge_4$, χT vs T decreases with decreasing temperature down to 0.45 K (not shown), suggesting the presence of antiferromagnetic correlations.

The M vs H in the magnetically ordered state of $Ce_2CoAl_7Ge_4$, $Ce_2NiAl_7Ge_4$, and $Ce_2IrAl_7Ge_4$ is shown in Fig. 4. $M(H)$ for $Ce_2CoAl_7Ge_4$ is linear up to 20 kOe and then bends over at higher fields, although it does not completely saturate up to 70 kOe. In $Ce_2NiAl_7Ge_4$ and $Ce_2IrAl_7Ge_4$, $M(H)$ exhibits a small hysteresis ($\sim$150 Oe for M = Ni and $\sim$400 Oe for M = Ir), characteristic of a soft ferromagnet. A ferromagneticlike state is consistent with a large value of $\chi(T)$ below 5 K for M = Ni, Ir, and is nearly an order of magnitude larger than that of $Ce_2CoAl_7Ge_4$ and $Ce_2PdAl_7Ge_4$. Furthermore, a plot of χT vs T (not shown) increases rapidly with decreasing temperature just above the ordering temperature, indicating the presence of ferromagnetic correlations in $Ce_2MAl_7Ge_4$ (M = Ni, Ir). At higher fields, the hysteresis is negligible in $Ce_2IrAl_7Ge_4$, and there are plateaus at 8, 16, and 24 kOe and a slope change at 50 kOe. The magnetic properties of $Ce_2MAl_7Ge_4$ (M = Co, Ni, Ir) in the magnetic field do not show typical behavior expected for a simple ferromagnet or antiferromagnet, suggesting these materials exhibit some form of complex magnetic ordering below 2 K, perhaps in an incommensurate magnetic state. This is consistent with neutron powder diffraction measurements well below T_M of $Ce_2CoAl_7Ge_4$ and $Ce_2NiAl_7Ge_4$, which found no evidence for additional peaks or extra intensity corresponding to magnetic ordering, within the instrument resolution. The magnetic moment per Ce in $Ce_2CoAl_7Ge_4$, $Ce_2IrAl_7Ge_4$, and $Ce_2NiAl_7Ge_4$ at the highest field measured of 70 kOe (Fig. 4) is 0.55, 1.2, and 0.9 μ_B, respectively. These values are much smaller than the free Ce^{3+} ion moment, given by $g_J J = 2.14\ \mu_B$. A reduction of the ordered moment in rare-earth systems may be due to crystal field effects and/or Kondo screening. $Ce_2PdAl_7Ge_4$ does not show any sign of magnetic ordering down to the lowest temperature measured (0.46 K).

C. Specific heat

The specific heat, plotted as C/T, for the $Ce_2MAl_7Ge_4$ compounds is shown in Figs. 5(a), 5(c), 5(e), and 5(g).

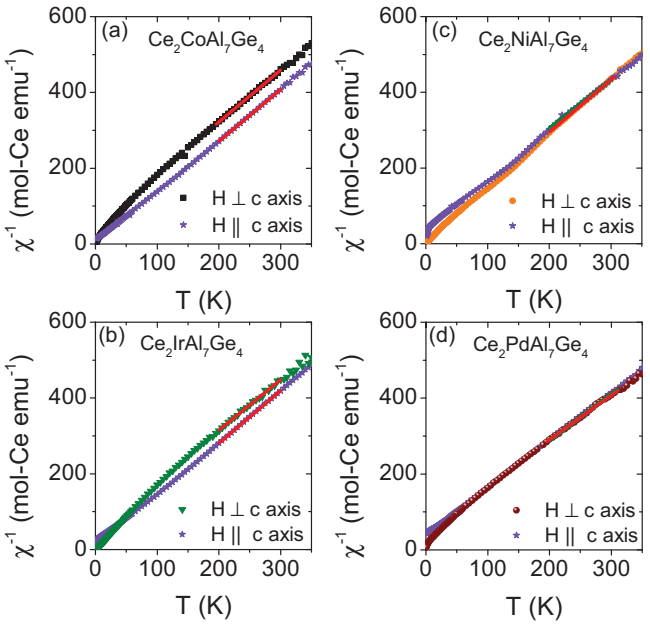

FIG. 3. Inverse magnetic susceptibility $\chi^{-1}(T)$ of $Ce_2MAl_7Ge_4$ (M = Co, Ni, Ir, Pd) measured in an external magnetic field of H = 1.1 kOe applied parallel and perpendicular to the crystallographic c axis. The solid line is a Curie-Weiss fit to the data.

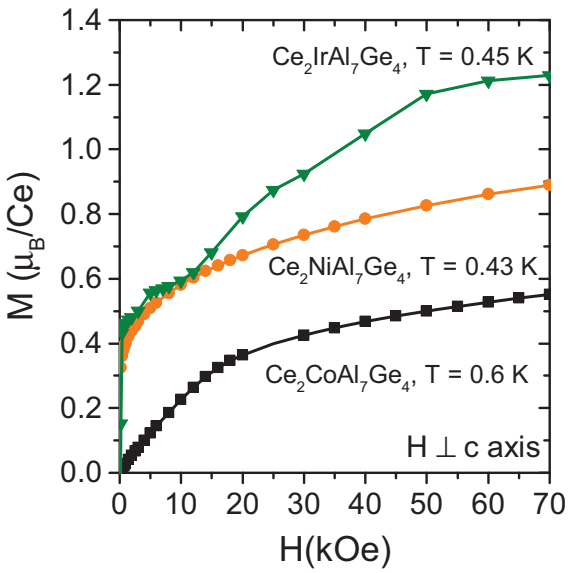

FIG. 4. M vs H of $Ce_2CoAl_7Ge_4$, $Ce_2IrAl_7Ge_4$, and $Ce_2NiAl_7Ge_4$, measured in the magnetically ordered state at the temperatures specified.

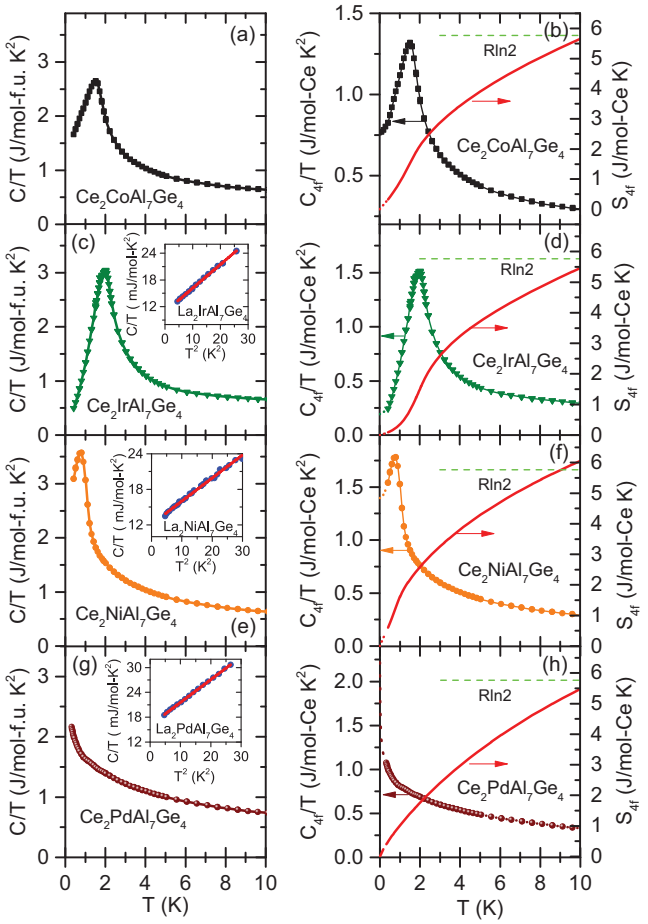

FIG. 5. Specific heat divided by temperature C/T as a function of temperature of (a) $Ce_2CoAl_7Ge_4$, (c) $Ce_2IrAl_7Ge_4$, (e) $Ce_2NiAl_7Ge_4$, and (g) $Ce_2PdAl_7Ge_4$. On the scale of these plots, C/T of the corresponding nonmagnetic, isostructural $La_2MAl_7Ge_4$ analogs is negligibly small. The insets show the low-temperature fit of the heat capacity of the La analogs. The right panels show the $4f$ contribution to the specific heat C_{4f}/T (left axis) and temperature evolution of the $4f$ contribution to the entropy S_{4f} (right axis) of (b) $Ce_2CoAl_7Ge_4$, (d) $Ce_2IrAl_7Ge_4$, (f) $Ce_2NiAl_7Ge_4$, and (h) $Ce_2PdAl_7Ge_4$. The dotted lines are an extrapolation of C_{4f}/T to $T = 0$ and are used to estimate the entropy below 0.4 K.

The $4f$ contribution to the heat capacity, plotted in Figs. 5(b), 5(d), 5(f), and 5(h), as C_{4f}/T is obtained by subtracting C/T of La counterparts $La_2MAl_7Ge_4$ from that of $Ce_2MAl_7Ge_4$. The $4f$ contribution to the entropy (S_{4f}), obtained by integrating C_{4f}/T with respect to T, also is shown in Figs. 5(b), 5(d), 5(f), and 5(h). The contribution of $La_2NiAl_7Ge_4$ was used to determine C_{4f}/T and S_{4f} of $Ce_2CoAl_7Ge_4$ because crystals of $La_2CoAl_7Ge_4$ were not grown. The La compounds show a behavior typical of a simple metal. The electronic contribution to the specific heat γ, obtained from a linear fit to C/T vs T^2 below 5.5 K of the form $C/T = \gamma + \beta T^2$ [insets in Figs. 5(c), 5(e), and 5(g)], are 10.8, 12.1, and 16.1 (mJ/mol f.u. K^2) for $La_2IrAl_7Ge_4$, $La_2NiAl_7Ge_4$, and $La_2PdAl_7Ge_4$, respectively.

The respective phonon specific heat coefficient β is 0.53, 0.51, and 0.40 (mJ/mol f.u. K^4). The Debye temperature estimated from β using the relation $\theta_D = \sqrt[3]{12\pi^4 r R/5\beta}$ (where r is number of atoms in the formula unit) for $La_2IrAl_7Ge_4$, $La_2NiAl_7Ge_4$, and $La_2PdAl_7Ge_4$ is 372, 412, and 367 K, respectively. A peak is observed in C/T signaling the onset of magnetic order at $T_M = 1.5$, 2.0, and 0.8 K in $Ce_2CoAl_7Ge_4$, $Ce_2IrAl_7Ge_4$, and $Ce_2NiAl_7Ge_4$, respectively. No peak is observed in $Ce_2PdAl_7Ge_4$ down to 0.4 K. Instead C/T increases with decreasing temperature down to 0.4 K, where it reaches a value of $\gamma = 1.0$ J/mol Ce K^2.

The entropy at the magnetic transition $S_{4f}(T_M)$ (per Ce) of $Ce_2CoAl_7Ge_4$, $Ce_2IrAl_7Ge_4$, and $Ce_2NiAl_7Ge_4$ is 0.27, 0.23, and 0.22 of $R\ln 2$, but the entropy of the CEF doublet ground state is recovered by ~10 K in the $Ce_2MAl_7Ge_4$ compounds [Figs. 5(b), 5(d), 5(f), and 5(h)]. Such a strong reduction of S_{4f} at T_M is expected when Kondo screening of the Ce moments occurs. A simple model relates the reduction of the specific heat jump at the magnetic transition $\Delta C(T_M)$ to the ratio of Kondo and ordering temperatures $T_K/T_{\rm mag}$ [26]. From a linear extrapolation of C/T from 10 K to T_M [Figs. 5(b), 5(d), 5(f), and 5(h)], the obtained peak heights $\Delta C \sim 1.0$, 1.6, and 1.0 J/mol Ce K for $Ce_2MAl_7Ge_4$, M = Co, Ir, Ni, respectively, are significantly reduced from the expected $\Delta C = 12.48$ J/mol Ce K for a $J = 1/2$ two-level magnetic system [26]. From these values of ΔC, we estimate that $T_K/T_{\rm mag} \sim 5$, 3, 5 for M = Co, Ir, Ni, respectively, yielding $T_K \sim 5$, 8, and 5 K. These values of T_K are in accord with the fact that the $4f$ entropy reaches $(1/2)R\ln 2$ at around 5 K in $Ce_2MAl_7Ge_4$, as expected from the calculations of Rajan [27]. Because C_{4f}/T increases over a broad temperature range as the magnetic transition is approached in the paramagnetic state, it is not possible to estimate accurately the electronic contribution to the specific heat (γ). Crudely, however, $\gamma \sim R\ln 2/T_K$, which implies that these are heavy-fermion systems with a Kondo temperature $T_K \sim 5$ K.

D. Electrical resistivity

Figure 6 shows the electrical resistivity of the $Ce_2MAl_7Ge_4$ compounds measured with current applied in the *ab* plane. In all four compounds, the electrical resistivity is weakly temperature dependent above 150 K. With decreasing temperature in $Ce_2CoAl_7Ge_4$, $Ce_2IrAl_7Ge_4$, and $Ce_2PdAl_7Ge_4$, a broad "knee" appears in $\rho(T)$ at around 100–150 K. Below 100 K, $\rho(T)$ of $Ce_2PdAl_7Ge_4$ passes through a distinct minimum at 45 K and a peak at 7 K, below which it drops sharply. $Ce_2CoAl_7Ge_4$ also shows a shallow minimum at 30 K and a peak at 10 K. In $Ce_2IrAl_7Ge_4$, the resistivity drops sharply below 20 K. $Ce_2NiAl_7Ge_4$ shows a shallow resistivity minimum at relatively higher temperature (200 K), below which resistivity gradually increases, making a peak at 4 K with a sharp drop below it. The three $Ce_2CoAl_7Ge_4$, $Ce_2IrAl_7Ge_4$, and $Ce_2NiAl_7Ge_4$ materials show a kink at the ordering temperature at $T_M = 1.8$, 1.8, and 0.8 K, respectively [inset of Figs. 6(a)–6(c)], in reasonable agreement with specific heat and magnetic susceptibility measurements. This feature is also reflected in the temperature derivative of resistivity $d\rho/dT$ as a peak [inset of Figs. 6(a)–6(c)]. No such feature is observed in $Ce_2PdAl_7Ge_4$, as expected from the susceptibility and heat capacity data.

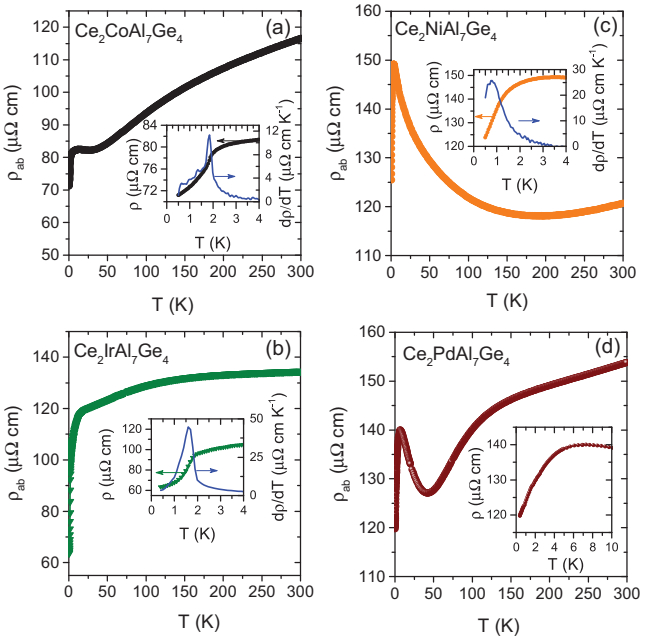

FIG. 6. Electrical resistivity as a function of temperature $\rho(T)$ with current applied in the ab plane of (a) $Ce_2CoAl_7Ge_4$, (b) $Ce_2IrAl_7Ge_4$, (c) $Ce_2NiAl_7Ge_4$, and (d) $Ce_2PdAl_7Ge_4$. The insets in (a–c) show the data between 0.4 and 4 K near the magnetic transition, along with the temperature derivative of the resistivity $d\rho/dT$. The inset in (d) shows the electrical resistivity of $Ce_2PdAl_7Ge_4$ between 0.4 and 10 K. The resistivity of $Ce_2CoAl_7Ge_4$ and $Ce_2NiAl_7Ge_4$ was measured in a small external magnetic field of 200 and 500 Oe, respectively.

The magnetoresistance (MR), defined as $[(\rho_H - \rho_0)/\rho_0] \times 100\%$, is depicted in Fig. 7 as a function of external magnetic field for the $Ce_2MAl_7Ge_4$ compounds measured with both the magnetic field and current applied in the ab plane in a transverse geometry. The MR of $Ce_2CoAl_7Ge_4$ at $T = 0.6$ K first increases with increasing magnetic field and shows a small jump at 2 kOe, goes through a maximum at 8.5 kOe, and then decreases with increasing H. It becomes negative at 28 kOe and saturates above 60 kOe. These features observed in MR correspond to features observed in M vs H measurements (Fig. 4). Although not clear in M vs H, dM/dH vs H (not shown) shows a decrease at 2 and 15 kOe. This MR behavior indicates that $Ce_2CoAl_7Ge_4$ does not have a metamagnetic transition up to 87 kOe. The MR of $Ce_2IrAl_7Ge_4$ at 0.4 K is more dramatic, with features at 7, 19, 36, and 50 kOe that closely follow those observed in M vs H (Fig. 4). At high fields, the MR is negative and saturates at–5% at 90 kOe. In $Ce_2NiAl_7Ge_4$, the magnetoresistance at 0.45 K decreases monotonically with increasing field up to 90 kOe, where it reaches a very large negative value of 43%. This behavior suggests that there are significant magnetic fluctuations in $Ce_2NiAl_7Ge_4$ at 0.45 K that are suppressed with a magnetic field, resulting in a large negative magnetoresistance. In contrast, the MR of $Ce_2PdAl_7Ge_4$ measured at 0.4 K increases with increasing H up to 70 kOe, then decreases slightly to 12.3% at 90 kOe.

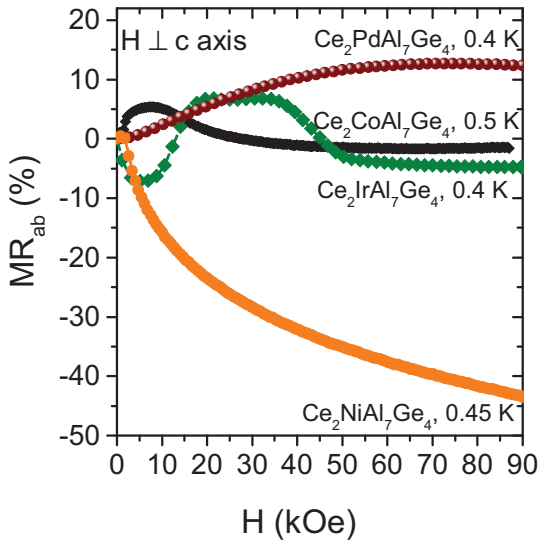

FIG. 7. Transverse magnetoresistance MR of $Ce_2MAl_7Ge_4$ with the current and the external magnetic field applied within the ab plane measured at the temperature specified.

E. Crystalline electric field analysis of $Ce_2PdAl_7Ge_4$

To better understand the interesting properties of $Ce_2PdAl_7Ge_4$ as well as to shed light on its crystal field scheme, we have analyzed the data presented in Fig. 8 using a model including interactions between nearest neighbors as well as the orthorhombic CEF Hamiltonian:

$$\mathcal{H} = J_{\rm AFM} \sum_{<i,l>} j_i \cdot j_l + B_2^0 O_2^0 + B_2^2 O_2^2 + B_4^0 O_4^0 + B_4^2 O_4^2 + B_4^4 O_4^4, \quad (1)$$

where $J_{\rm AFM} > 0$ represents an AFM interaction between nearest-neighbor local spins j_i, B_i^n are the CEF parameters, and O_i^n are the Stevens equivalent operators obtained from the angular momentum operators [28,29]. The first term in the Hamiltonian in Eq. (1) may be simplified to $zJj \cdot \langle j \rangle$ via a mean-field approximation ($j_i \cdot j_l \sim j \cdot \langle j \rangle$), where z is the number of nearest neighbors. Although $\mathcal{H}$ may be solved by this approach, the best fits to the data are achieved when a second antiferromagnetic exchange interaction $J'_{\rm AFM}$ is included, which agrees with the results from the Curie-Weiss fits at high temperatures. This model was then used to simultaneously fit $\chi(T)$ in the whole temperature range, $M(H)$ at 2.5 K and C/T with $T > 16$ K as a constraint, yielding the CEF parameters as well as the antiferromagnetic $RKKY$ exchange parameters displayed in Table V. When $B_2^0 > 0$, the Stevens operator $O_{2,i}^0 = 3\hat{J}_{z,i}^2 - J(J+1)$ favors in-plane alignment of spins (i.e., $\hat{J}_z = 0$), which is consistent

TABLE V. Extracted crystal field parameters (in Kelvin) for $Ce_2PdAl_7Ge_4$. Here, $z_{\rm AFM}$ is the number of nearest neighbors with AFM coupling.

	B_2^0	B_2^2	B_4^0	B_4^2	B_4^4	$z_{\rm AFM}J_{\rm AFM}$	$z'_{\rm AFM}J'_{\rm AFM}$
$Ce_2PdAl_7Ge_4$	1.79	–0.53	0.24	0.016	2.49	0.87	0.52

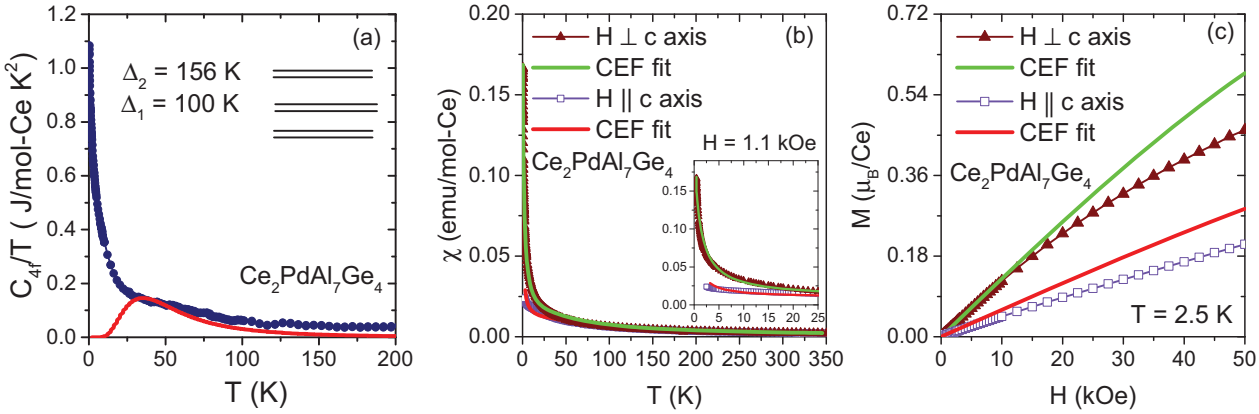

FIG. 8. (a) Fits of a CEF model to the (a) heat capacity, (b) magnetic susceptibility, and (c) magnetization data of $Ce_2PdAl_7Ge_4$. Inset in (b) shows χ vs T below 25 K.

with the magnetic susceptibility data ($\chi_{ab} > \chi_c$). In fact, there is good agreement between the fits and the experimental $\chi(T)$ data [Fig. 8(b)]. The $M(H)$ data at 2.5 K, however, cannot be exactly reproduced, as shown in Fig. 8(c), although the anisotropy and the shape of the magnetization fits are reasonable. The observed discrepancy likely arises from the fact that the model is an approximation that takes into account only single-ion CEF effects and mean-field interactions, which mimic $RKKY$ interactions, and does not include any additional effects from the Kondo interactions and/or quantum fluctuations. Thus, although there is good agreement at high temperatures, the CEF model should not be expected to account for the low-temperature properties of $Ce_2PdAl_7Ge_4$ discussed below.

The extracted parameters resulted in the CEF level scheme shown in Fig. 8(a) for $Ce_2PdAl_7Ge_4$ and are summarized in Table VI. The ground-state doublet is separated from the first excited state and the second excited state by 100 K and 156 K, respectively. We note that the obtained CEF scheme can reproduce the main features of the data shown in Fig. 8, i.e., the Schottky anomaly and the magnetic anisotropy. A broad feature in the electrical resistivity at ~125 K is also consistent with scattering associated with depopulation of the excited CEF levels. If this is the case, then a similar CEF scheme might be expected for $Ce_2CoAl_7Ge_4$ and $Ce_2IrAl_7Ge_4$ (although it is less clear in $Ce_2NiAl_7Ge_4$). In addition, the exchange interactions are small (<1 K) and suggest the presence of antiferromagnetic interactions at low temperature. Nevertheless, it is important to emphasize that the CEF parameters obtained from fits to macroscopic measurements may not be unique and/or extremely precise. An accurate determination of the CEF scheme and its parameters requires a direct measurement by, for example, inelastic neutron scattering [30], or the mixing parameters of the ground-state wave function may be obtained from x-ray absorption studies [31].

TABLE VI. Energy levels and wave functions of the CEF scheme obtained from the thermodynamic properties of $Ce_2PdAl_7Ge_4$.

	Energy levels and wave functions					
$E(K)$	$\|-5/2\rangle$	$\|-3/2\rangle$	$\|-1/2\rangle$	$\|+1/2\rangle$	$\|+3/2\rangle$	$\|+5/2\rangle$
156	–0.87	–0.015	0.041	0.0012	–0.495	–0.025
156	–0.025	0.495	0.0012	–0.041	0.015	0.87
100	–0.006	0.006	–0.13	0.99	0.0	0.04
100	0.04	0.0	0.99	0.13	0.006	0.006
0	–0.089	0.85	0.003	0.016	0.16	–0.49
0	–0.49	–0.16	0.016	–0.003	0.85	0.089

IV. DISCUSSION

Among the four compounds studied, $Ce_2CoAl_7Ge_4$, $Ce_2NiAl_7Ge_4$, $Ce_2IrAl_7Ge_4$, and $Ce_2PdAl_7Ge_4$, the first three show clear magnetic ordering below 2 K in susceptibility, resistivity, and heat capacity measurements. The magnetic structure of these compounds appears to be complex, as suggested by the lack of any additional signal of magnetic order in powder neutron diffraction below T_M in the M = Co and Ni compounds and the multiple features in the $M(H)$ curve in the ordered state of the M = Ir compound. The apparent ferromagneticlike and antiferromagnetic ordered states in $Ce_2MAl_7Ge_4$ (M = Co, Ni, Ir) suggest a finely tuned balance of competing magnetic exchange interactions. It is possible that these compounds have an incommensurate magnetic structure or that the ordered moment is too small to be detected within the resolution of the neutron powder diffraction experiment. The low ordering temperatures, the reduced specific heat jumps at T_M, and the small amount of entropy released below T_M (~25% of $R\ln 2$) uniformly point to the $Ce_2MAl_7Ge_4$ compounds being close to a magnetic/nonmagnetic boundary in the Doniach diagram. $Ce_2PdAl_7Ge_4$ may be very close to this boundary, as it does not show any sign of magnetic ordering down to 0.4 K. Instead, it exhibits non-Fermi liquid behavior as shown in Fig. 9. $C_{4f}(T)/T$ follows a $\sim -\ln(T)$ temperature dependence between 0.4 K and 18 K [Fig. 9(a)]. Upon application of an in-plane magnetic field of 10 kOe, the logarithmic behavior deviates below 0.8 K [inset of Fig. 9(a)]. In addition, the resistivity is linear in temperature $\rho \sim T$ between 0.4 K and 1.8 K [Fig. 9(b)]. In magnetic field, the low-temperature resistivity deviates from T-linear behavior. At 10 kOe, fits of $\rho(T) = \rho_0 + AT^n$ to the data between $0.4 < T < 1.8$ yield $n = 1.4$ [left inset in Fig. 9(b)] and exhibits Fermi liquid T^2

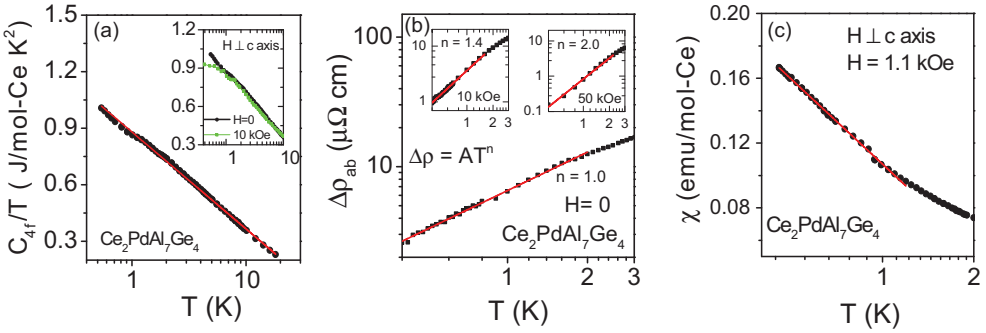

FIG. 9. (a) C_{4f}/T vs T of $Ce_2PdAl_7Ge_4$ on a semilog plot. The inset shows C_{4f}/T measured in $H = 0$ and 10 kOe, applied parallel to the ab plane. (b) Log-log plot of $\triangle\rho$ vs T of $Ce_2PdAl_7Ge_4$ between 0.4 and 3 K for $H = 0$ (main panel), 10 kOe (left inset), and 50 kOe (right inset). $\triangle\rho = \rho - \rho_0$, ρ_0 is the extrapolated ρ at $T = 0$. The solid lines are the power law ($\triangle\rho = AT^n$) fits to the data. The magnetic field was applied parallel to the ab plane. (c) χ vs T of $Ce_2PdAl_7Ge_4$ on a semilog plot. In the main panels, the solid line is a linear fit to the data.

behavior at 50 kOe below 2.4 K [right inset in Fig. 9(b)]. Figure 9(c) shows the magnetic susceptibility of $Ce_2PdAl_7Ge_4$ on a semilog plot. Between 0.4 K and 1 K, $\chi(T) \sim -\ln(T)$. All these properties suggest that in the normal state $Ce_2PdAl_7Ge_4$ shows NFL behavior at the lowest temperature measured (0.4 K), with the application of a magnetic field driving the system towards a Fermi liquid state. It will be interesting to see if $Ce_2PdAl_7Ge_4$ is right at the quantum critical point with non-Fermi liquid properties extending to temperatures below 0.4 K, or whether it is just away from the QCP and either orders magnetically or is a Fermi liquid at very low temperatures. These lower temperature measurements may also allow a better understanding of the nature of the quantum fluctuations and which theoretical models [4,32–34] might be appropriate for describing this system. Pressure measurements on the other magnetically ordered $Ce_2MAl_7Ge_4$ compounds, in which pressure is expected to tune the system towards the magnetic/nonmagnetic boundary, would also be worthwhile.

V. SUMMARY

Single crystals of the compounds $Ce_2MAl_7Ge_4$ (M = Co, Ir, Ni, Pd) were synthesized and their physical properties were determined by means of x-ray and neutron diffraction, magnetic susceptibility, specific heat, and electrical resistivity measurements. These compounds crystallize in a noncentrosymmetric tetragonal space group $P\bar{4}2_1m$. $Ce_2CoAl_7Ge_4$, $Ce_2NiAl_7Ge_4$, and $Ce_2IrAl_7Ge_4$ order magnetically below 2 K. $Ce_2PdAl_7Ge_4$ does not show magnetic ordering down to 0.4 K. An analysis of heat capacity data suggests that these materials are heavy-fermion compounds with a Kondo scale of order $T_K \sim$ 5–8 K that is comparable to the ordering temperatures, placing them close to a magnetic/nonmagnetic boundary. $Ce_2PdAl_7Ge_4$ shows NFL behavior and appears to be at, or close to, a quantum critical point.

ACKNOWLEDGMENTS

We thank Z. Fisk, J. Lawrence, and A. Mar for stimulating discussion. Work at Los Alamos National Laboratory was performed under the auspices of the U.S. Department of Energy, Office of Basic Energy Sciences, Division of Materials Sciences and Engineering. The EDS measurements were performed at the Center for Integrated Nanotechnologies, an Office of Science User Facility operated for the U.S. Department of Energy (DOE) Office of Science. Los Alamos National Laboratory, an affirmative action equal opportunity employer, is operated by Los Alamos National Security, LLC, for the National Nuclear Security Administration of the U.S. Department of Energy under Contract No. DE-AC52-06NA25396. P.F.S.R. acknowledges a Director's Postdoctoral Fellowship supported through the Los Alamos LDRD program. Support for T.E.A.S. and S.K.C. was provided by the Chemical Sciences, Geosciences, and Biosciences Division, Office of Basic Energy Sciences, Office of Science, Heavy Elements Chemistry Program, U.S. Department of Energy, under Grant No. DE-FG02-13ER16414. Y.L. was supported by the Institute of Basic Sciences (IBS), Grant No. IBS-R014-D1. We acknowledge the support of the National Institute of Standards and Technology, U.S. Department of Commerce, in providing the neutron research facilities used in this work.

APPENDIX: ATOMIC COORDINATES AND EQUIVALENT DISPLACEMENT PARAMETERS OF $Ce_2MAl_7Ge_4$

TABLE VII. Atomic coordinates and equivalent displacement parameters (Å^2) for $Ce_2IrAl_7Ge_4$ determined by single-crystal x-ray diffraction at room temperature. U_{eq} is defined as one-third of the trace of the orthogonalized U^{ij} tensor.

Atom	Wyckoff	Occ.	x	y	z	U_{eq}
Ir(1)	2a	1	0	0	0	0.005(1)
Ce(1)	4d	1	0	0	–0.2584(1)	0.007(1)
Ge(1)	2c	1	0.5	0	–0.2026(1)	0.008(1)
Ge(2)	2c	1	0	0.5	–0.1917(1)	0.007(1)
Ge(3)	4e	1	0.2806(1)	–0.2194(1)	–0.4132(1)	0.011(1)
Al(1)	4e	1	–0.2946(3)	–0.2054(3)	–0.4277(2)	0.007(1)
Al(2)	2c	1	0	–0.5	–0.3555(2)	0.010(1)
Al(3)	4e	1	–0.2559(2)	–0.2441(2)	–0.0867(3)	0.008(1)
Al(4)	4e	1	–0.7439(2)	–0.2439(2)	–0.0872(3)	0.007(1)

TABLE VIII. Atomic coordinates and equivalent displacement parameters (Å^2) for $Ce_2NiAl_7Ge_4$ determined by single-crystal x-ray diffraction at room temperature. U_{eq} is defined as one-third of the trace of the orthogonalized U^{ij} tensor.

Atom	Wyckoff	Occ.	x	y	z	U_{eq}
Ni(1)	2*a*	1	0	0	0	0.005(1)
Ce(1)	4*d*	1	0	0	–0.2588(1)	0.006(1)
Ge(1)	2*c*	1	0.5	0	–0.1996(1)	0.007(1)
Ge(2)	2*c*	1	0	0.5	–0.1884(1)	0.006(1)
Ge(3)	4*e*	1	0.2798(1)	–0.2202(1)	–0.4130(1)	0.009(1)
Al(1)	4*e*	1	–0.2936(2)	–0.2064(2)	–0.4273(1)	0.007(1)
Al(2)	2*c*	1	0	-0.5	–0.3544(1)	0.010(1)
Al(3)	4*e*	1	–0.2557(2)	–0.2443(2)	–0.0851(2)	0.007(1)
Al(4)	4*e*	1	–0.7436(2)	–0.2436(2)	–0.0852(2)	0.008(1)

TABLE IX. Atomic coordinates and equivalent displacement parameters (Å^2) for $Ce_2PdAl_7Ge_4$ determined by single-crystal x-ray diffraction at room temperature. U_{eq} is defined as one-third of the trace of the orthogonalized U^{ij} tensor.

Atom	Wyckoff	Occ.	x	y	z	U_{eq}
Pd(1)	2*a*	1	0	0	0	0.004(1)
Ce(1)	4*d*	1	0	0	–0.2611(1)	0.005(1)
Ge(1)	2*c*	1	0.5	0	–0.2031(1)	0.007(1)
Ge(2)	2*c*	1	0	0.5	–0.1906(1)	0.008(1)
Ge(3)	4*e*	1	0.2796(1)	–0.2204(1)	–0.4139(1)	0.009(1)
Al(1)	4*e*	1	–0.2974(3)	–0.2026(3)	–0.4269(1)	0.005(1)
Al(2)	2*c*	1	0	–0.5	–0.3572(2)	0.007(1)
Al(3)	4*e*	1	–0.2562(2)	–0.2438(2)	–0.0890(3)	0.007(1)
Al(4)	4*e*	1	–0.7430(2)	–0.2430(2)	–0.0895(4)	0.008(1)

[1] G. R. Stewart, Rev. Mod. Phys. **56**, 755 (1984).
[2] Z. Fisk, D. W. Hess, C. J. Pethick, D. Pines, J. L. Smith, J. D. Thompson, and J. O. Willis, Science **239**, 33 (1988).
[3] S. Doniach, Physica B and C **91**, 231 (1977).
[4] H. v. Löhneysen, A. Rosch, M. Vojta, and P. Wölfle, Rev. Mod. Phys. **79**, 1015 (2007).
[5] S. Sachdev, *Quantum Phase Transitions* (Cambridge University Press, Cambridge, 2011).
[6] O. Stockert and F. Steglich, Annu. Rev. Condens. Matter Phys. **2**, 79 (2011).
[7] P. Monthoux, D. Pines, and G. G. Lonzarich, Nature (London) **450**, 1177 (2007).
[8] C. Pfleiderer, Rev. Mod. Phys. **81**, 1551 (2009).
[9] J. D. Thompson, M. Nicklas, A. Bianchi, R. Movshovich, A. Llobet, W. Bao, A. Malinowski, M. F. Hundley, N. O. Moreno, P. G. Pagliuso *et al.*, Phys. B (Amsterdam, Neth.) **329-333**, 446 (2003).
[10] E. Bauer and M. Sigrist, *Non-Centrosymmetric Superconductors: Introduction and Overview* (Springer, Heidelberg, 2012).
[11] A. Szytula and J. Leciejewicz, *Handbook of Crystal Structures and Magnetic Properties of Rare Earth Intermetallics* (CRC Press, Boca Raton, FL, 1994).
[12] K. Lejaeghere, G. Bihlmayer, T. Björkman, P. Blaha, S. Blügel, V. Blum, D. Caliste, I. E. Castelli, S. J. Clark, A. D. Corso *et al.*, Science **351**, aad3000 (2016).
[13] C.-K. Skylaris, Science **351**, 1394 (2016).
[14] N. J. Ghimire, F. Ronning, D. J. Williams, B. L. Scott, Yongkang Luo, J. D. Thompson, and E. D. Bauer, J. Phys.: Condens. Matter **27**, 025601 (2015).
[15] N. J. Ghimire, S. Calder, M. Janoschek, and E. D. Bauer, J. Phys.: Condens. Matter **27**, 245603 (2015).
[16] A. Maurya, R. Kulkarni, A. Thamizhavel, D. Paudyal, and S. K. Dhar, J. Phys. Soc. Jpn. **85**, 034720 (2016).
[17] Unit conversions: Oe to ampere per meter (A/m) multiply by 7.957 (747×10^1; molar magnetic susceptibility $= MV_m/H$, where V_m is the volume per gram mole; 1 emu/(mol Oe) $= 4\pi \times 10^{-6}$ m^3/mol.
[18] J. Rodriguez-Carvajal, Phys. B (Amsterdam, Neth.) **192**, 55 (1993).
[19] B. W. Roberts, J. Phys. Chem. Ref. Data **5**, 581 (1976).
[20] X. Z. Chen, P. Small, S. Sportouch, M. Zhuravleva, P. Brazis, C. R. Kannewurf, and M. G. Kanatzidis, Chem. Mater. **12**, 2520 (2000).
[21] J. Y. Cho, J. N. Millican, C. Capan, D. A. Sokolov, M. Moldovan, A. B. Karki, D. P. Young, M. C. Aronson, and J. Y. Chan, Chem. Mater. **20**, 6116 (2008).
[22] R. T. Macaluso, J. N. Millican, S. Nakatsuji, H.-O. Lee, B. Carter, N. O. Moreno, Z. Fisk, and J. Y. Chan, J. Solid State Chem. **178**, 3547 (2005).
[23] A. L. Spek, J. Appl. Crystallogr. **36**, 7 (2003).
[24] CIFs have been deposited with the Fachinformationszentrum Karlsruhe, 76344 Eggenstein-Leopoldshafen, Germany (Fax: (49)7247-808-666; Email: crysdata@fiz.karlsruhe.de), depository numbers CSD-430139 for $Ce_2IrAl_7Ge_4$, CSD-430140 for $Ce_2CoAl_7Ge_4$, CSD-430141 for $Ce_2PdAl_7Ge_4$, and CSD-430142 for $Ce_2NiAl_7Ge_4$.
[25] J. L. C. Daams and P. Villars, J. Alloys Compd. **252**, 110 (1997).
[26] M. J. Besnus, A. Braghta, N. Hamdaoui, and A. Meyer, J. Magn. Magn. Mater. **104-107**, 1385 (1992).
[27] V. T. Rajan, Phys. Rev. Lett. **51**, 308 (1983).
[28] M. T. Hutchings, *Solid State Physics: Advances in Research and Applications*, edited by F. Seitz and B. Turnbull (Academic Press, New York, 1964), Vol. 16, p. 227.
[29] K. W. H. Stevens, Proc. Phys. Soc., London, Sect. A **65**, 209 (1952).
[30] E. A. Goremychkin and R. Osborn, Phys. Rev. B **47**, 14280 (1993).
[31] T. Willers, Z. Hu, N. Hollmann, P. O. Körner, J. Gegner, T. Burnus, H. Fujiwara, A. Tanaka, D. Schmitz, H. H. Hsieh, H.-J. Lin, C. T. Chen, E. D. Bauer, J. L. Sarrao, E. Goremychkin, M. Koza, L. H. Tjeng, and A. Severing, Phys. Rev. B **81**, 195114 (2010).
[32] Q. Si, S. Rabello, K. Ingersent, and J. L. Smith, Nature (London) **413**, 804 (2001).
[33] C. Pépin, Phys. Rev. Lett. **98**, 206401 (2007).
[34] E. Abrahams and P. Wölfle, Proc. Natl. Acad. Sci. USA **109**, 3238 (2012).